International Journal of Solids and Structures 46 (2009) 3323–3335

Contents lists available at ScienceDirect

International Journal of Solids and Structures

journal homepage: www.elsevier.com/locate/ijsolstr

Grain boundary response of aluminum bicrystal under micro scale laser shock peening

Siniša Vukelić *, Jeffrey W. Kysar, Y. Lawrence Yao

Mechanical Engineering Department, Columbia University, New York, NY 10027, USA

ARTICLE INFO

Article history:
Received 26 November 2008
Received in revised form 18 April 2009
Available online 6 May 2009

Keywords:
Laser shock peening
Bicrystal
Plasticity

ABSTRACT

Micro scale laser shock peening (μLSP) is a process in which compressive residual stresses are induced in a material surface to improve fatigue life and wear resistance under cyclic loading. Since the diameter of the laser spot used during the process is the same order of magnitude as grain size, the effects of anisotropy and heterogeneity have to be explicitly taken into account in any model of the process. In this study experimental and numerical studies have been performed in order to investigate the response of an aluminum bicrystal under laser shock peening. The grain boundary is shocked to investigate heterogeneity, and single crystals are shocked to study the effect of anisotropy in the absence of heterogeneity. The orientations of the crystals in the bicrystal as well as the reference single crystals have been chosen such that an approximate plane strain condition is achieved. A finite element model which accounts for the anisotropy, heterogeneity and inertia has also been developed based on single crystal micromechanics. Simulation results are compared with experimental findings. The potential benefit of μLSP as a surface treatment for improvement of fatigue life is also discussed.

1. Introduction

Laser shock peening (LSP) as a process of surface properties enhancement (Clauer and Holbrook, 1981; Clauer and Lahrman, 2001) was introduced in 1960s as a potential replacement for conventional shot peening (Curtis et al., 2002). Both LSP and conventional shot peening induce compressive residual stresses of the same order of magnitude which improve material properties of various metals such as copper, nickel, aluminum, etc. (Hammersley et al., 2000) under cyclic loading. However, the use of laser shocking rather than the bombardment of a surface with hard particles has a number of advantages which include: deeper shock wave penetration as well as a significant increase in process flexibility with respect to the potential geometries of treated areas. On the other hand, the high cost of lasers powerful enough to produce beam spot size of the order of millimeters with power densities of several GW/cm^2 has prevented wider industry application of LSP.

The development of micron size devices like micro electromechanical systems (MEMS), micro switches, etc. has raised the issue of improvement of reliability of these components. In order to improve its fatigue life and wear resistance, micro scale laser shock peening (μLSP) has been developed (Zhang and Yao, 2002) which employs a laser beam spot size of approximately 10 μm. The surface of interest is coated with a thin coating of aluminum foil or paint to protect the surface from thermal effects and thus to prevent change in microstructure due to high temperatures. The upper portion of ablative coating becomes plasma during the process which induces a pressure shock that propagates into the material and mechanically alters the residual stress distribution (Chen et al., 2004a,b). At first, most of the studies of μLSP involved polycrystalline materials (Zhang and Yao, 2002). However, because of the fact that the laser beam diameter size is of the same order of magnitude as the average size of grains in typical aluminum and copper so that deformation is expected to be induced in only a few grains. Therefore the material properties must be assumed to be anisotropic and inhomogeneous, which motivates the current line of research. The study of anisotropy effects on μLSP has been performed using individual single crystals of aluminum and copper by Chen et al. (2004a,b), Wang et al. (2008) and Vukelić et al. (2009a). In order to further understand the effect of anisotropy, the response of two different orientations of single crystal aluminum have been compared (Vukelić et al., 2009a) to analyze the difference between single and double slip cases.

The grain size plays a very important role in the mechanical behavior of polycrystalline metals. Therefore it is of interest to investigate interaction between grains. The well-known Hall–Petch effect (Hall, 1951, Petch, 1953) establishes a relationship between grain size and yield stress due to the fact that grain boundaries serve as obstacles to the motion of dislocations, causing them to pile up at the boundary resulting in a stress concentration that

* Corresponding author. Tel./fax: +1 212 666 2393.
E-mail address: sv2147@columbia.edu (S. Vukelić).

0020-7683/$ - see front matter © 2009 Elsevier Ltd. All rights reserved.
doi:10.1016/j.ijsolstr.2009.04.021

increases the required stress for activation of dislocation sources. Livingston and Chalmers (1957) employed iso-axial aluminum bicrystals to study the process of secondary slip activation. Heterogeneity in plastic deformation was further analyzed by Rey and Zaoui (1979) who considered the geometrical aspects of slip heterogeneities in aluminum bicrystals and made comparison with the single crystal response. These studies were predominantly experimental and involved tensile tests and examination of free surfaces. Hook and Hirth (1967) examined Fe–3%Si alloy bicrystals to investigate the influence of plastic and elastic incompatibility on stress concentrations at the grain boundary. Their study involved analysis of dislocation structure in the interior.

More recent studies focused on fundamental aspects of grain boundary mechanics. Mesarevic and Kysar (1996) analyzed dislocation nucleation and crack growth at the boundary of Cu/Al_2O_3 bicrystals. They described the crack tip stress field under quasistatic loading under plane strain conditions, analytical and numerically using 'small strain', finite deformation and ideal plasticity formulations. Kysar (2000) analyzed the directional crack growth dependence at the interface of a copper/sapphire bicrystal. The investigation included finite element analysis and experimental results with an extensive review of single crystal plasticity. Evers et al. (2002) developed a model which divides a grain into two parts: a core and several bicrystal boundaries. In that work it is stated that heterogeneous deformation between core and boundaries initiates the development of geometrically necessary dislocations (GNDs) to maintain lattice compatibility. Furthermore according to this approach, the newly created GNDs prevent dislocation motion which results in enhanced hardening. Another model based on GNDs is proposed by Ma et al. (2006) and examines the interaction between dislocations and grain boundaries from the theoretical and experimental point of view under a simple shear test. Wei and Anand (2004) discussed the effects of grain boundary sliding and separation in polycrystalline nickel. They coupled a single crystal plasticity model of a grain interior with an elastic–plastic grain boundary interface model. Moreover they developed a numerical model for a qualitative study of deformation and fracture of nanocrystalline nickel in simple tension.

The purpose of the present study is to examine the effect of heterogeneity under μLSP through numerical and experimental work. A finite element model is developed to investigate the response of an aluminum bicrystal under Gaussian pressure loading and a series of experiments are conducted for comparison. The benefit of μLSP as a surface treatment for improvement of fatigue life will also be discussed.

2. Experimental setup

2.1. Sample preparation

In this study an aluminum bicrystal grown from the melt was used. It was mounted on a three circle goniometer and the orientations of its crystals were determined using Laue diffraction to within ±1°. It is a symmetric tilt-type grain boundary with the [1 1 0] direction in both crystals parallel to the tilt axis of the adjoining grains, as seen in Fig. 1. The specimen was cut from the as-grown bicrystal using a wire electro-discharge machine (EDM) to 46 mm long, 11.6 mm wide and 7.7 mm high. The typical thickness in most MEMS applications is much smaller than the one in our specimen. However, the aim of this paper is fundamental research and study of effects of heterogeneity and anisotropy in semi-infinite conditions. The MEMS applications are referred as ones that can potentially benefit from this investigation in future. The surfaces of the individual crystals to be shocked deviated about 9.5° and 2.5°, respectively, from the ideal (1 1 0) and (0 0 1) surfaces. The sample was later mechanically polished in order to remove the heat affected zone (HAZ), followed by electropolishing to remove any remaining residually stressed material. The bicrystal was afterwards etched with a solution of sodium hydroxide and deionized water for about two minutes to reveal the grain boundary along which laser shocks were to be applied. After shocking and subsequent characterization of the top surface were completed, the specimen was sectioned using the EDM in order to examine the cross-section. The same polishing procedure was then applied to the cross-section.

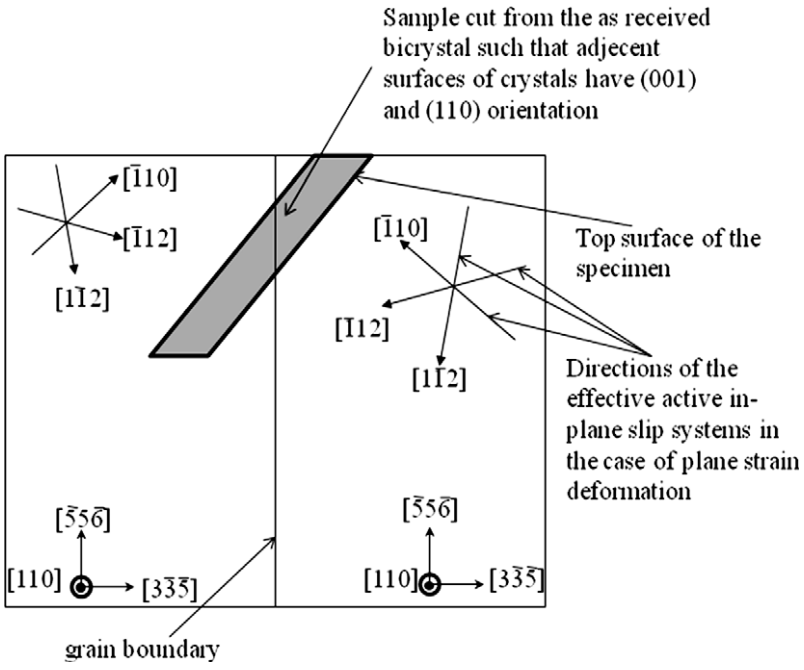

Fig. 1. Bicrystal grown from melt.

2.2. Shocking

A frequency tripled Q-switched Nd:YAG laser with wavelength λ = 355 nm in TEM_{00} mode was used for the μLSP experiments. The beam diameter was 12 μm and the pulse duration was 50 ns with approximate laser pulse energy of 320 μJ. The specimen was placed in a shallow container mounted on a computer-controlled Aerotech motorized linear stage where the laser beam path was carefully aligned with the grain boundary. Since the diameter of the laser beam is at least four orders of magnitude larger than the width of the grain boundary it is expected that laser shocks were placed either on the boundary or very close to it along the entire shock line. After alignment, a thin layer of vacuum grease was spread on the top surface and a 16 μm thick polycrystalline aluminum foil was applied to serve as an ablation layer in order to prevent thermal effects from reaching the surface of the bicrystal. The container was then filled with distilled water which was used as a confining medium and laser shocks were applied with 25 μm spacing. The overall experimental setup is illustrated in Fig. 2. A similar procedure was followed for laser shocking of reference single crystals away from the grain boundary. More details about laser shocking can be found at Zhang and Yao (2002), Chen et al. (2004a,b) and Vukelić et al. (2009a,b). Approximate two-dimensional deformation in FCC single crystals can be achieved if line loading is applied parallel to the (1 1 0) direction as discussed in Rice (1987), Kysar et al. (2005), Crone et al. (2004). It is well known that six active slip systems specify arbitrary stress state. The assumption of constant volume for plastic strain reduces the number of independent plastic strain components to five. When single laser shock applied onto the (1 1 0) or (0 0 1) surface of a FCC single crystal only four slip systems will be activated (Chen et al., 2007). Rice (1987) has shown that these four slip systems form two effective slip systems which are activated in equal amounts. Chen et al. (2007) has shown that shock loading generates predominantly plane strain deformation state in (1 1 0) plane.

2.3. Characterization

Prior to shock peening, the surface roughness of the sample was measured using an atomic force microscope (AFM), in order to establish the baseline roughness and determine the influence of etching on the bicrystal grain boundary. After shocking, the geometry of the affected region was characterized using a profilometer. In addition, the size of the plastically deformed region was estimated by characterizing the region over which significant crystal lattice rotation occurred (Kysar and Briant, 2002; Wang et al., 2008; Vukelić et al., 2009a). For this purpose Electron Backscatter Diffraction (EBSD) was employed to spatially map the crystallographic orientation as a function of position along the shocked surface using a JEOL JSM 5600LV scanning electron microscope with HKL Technology EBSD system. Crystallographic orientations were determined over regions with extents of 190 μm × 285 μm and 120 μm × 240 μm on the top surface and cross-section, respectively. A similar procedure was carried out for characterizing the reference single crystals.

3. Numerical model

The bicrystal model developed in this work is decomposed into the single crystal interior and grain boundary. Crystal plasticity theory developed by Hill (1950), Rice (1973, 1987), Asaro (1983) and Asaro and Needleman (1985) is applied to the grain interiors. According to this theory plastic deformation occurs on slip systems described by slip directions and slip normals. Single crystal plasticity theory assumes that the deformation gradient tensor can be multiplicatively decomposed into two components, one responsible for plastic shear on all potentially active slip systems and the other for elastic strain and lattice rotation, as illustrated at Fig. 3. Therefore, the measured lattice rotation is a consequence of the rotation due to the elastic portion of the deformation gradient tensor. In this way all the effects of finite deformation can be incorporated into the theory. It is assumed that there is no influence of temperature effects although it is expected that material would heat up during the sequentially applied laser shocks. This phenomenon and its influence on deformation state will be subject of future study. The grain boundary is assumed to be rigid, neither debonding nor sliding is allowed to occur. Such an assumption discounts the potential of grain boundary deformation. However, since the applied loads on the grain boundary are highly compressive, no debonding is expected to occur, however the potential for grain boundary sliding and debonding is a suitable topic for further research.

The analysis is performed with the commercial finite element (FEM) program ABAQUS/Standard with User Defined Material subroutine (UMAT), based on single crystal plasticity theory

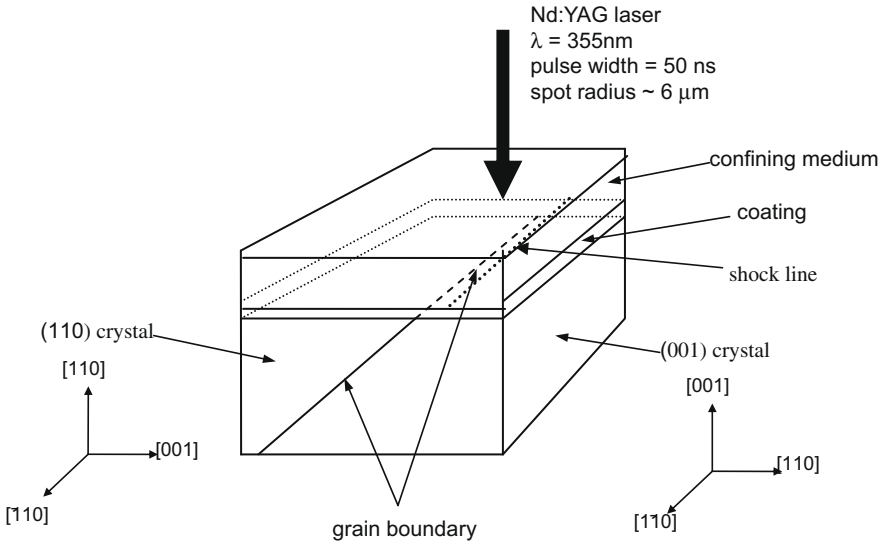

Fig. 2. Experimental setup.

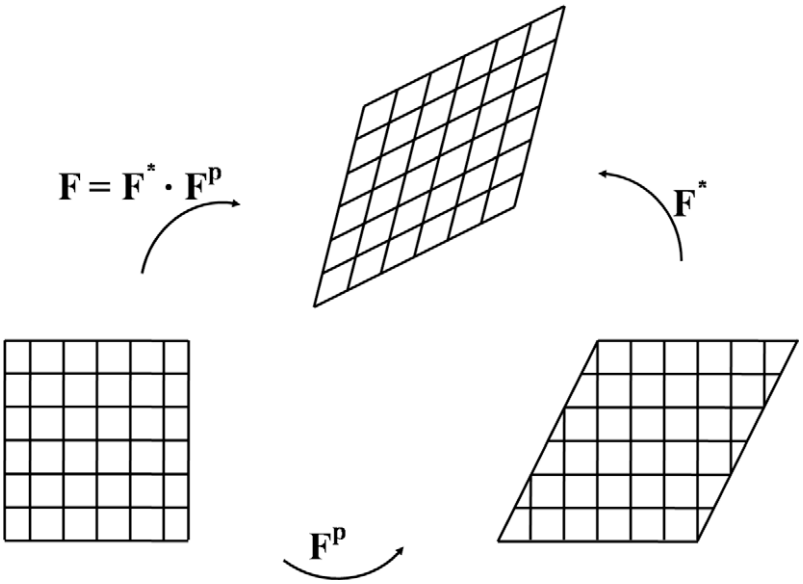

Fig. 3. Single crystal plasticity – lattice rotation and slip.

formulated by Asaro (1983), written by Huang (1991) and modified by Kysar (1997). The mesh consists of two-dimensional 4-noded quadrilateral elements with reduced integration. The crystallographic orientation relative to the finite element mesh is chosen such that plane strain is achieved in the plane of (1 1 0) (Rice, 1987; Kysar, 2000). Pressure applied on the interface of two different surfaces, (0 0 1) and the $(1\,\bar{1}\,0)$. Boundaries are modeled with semi-infinite elements and therefore there are no reflections of the elastic waves once they propagate through the domain of interest. The pressure loading $P(x,t)$ is dynamic and has spatial and temporal component embedded into it. The spatial component follows a Gaussian distribution pressure

$$P(x) = P_0(t)\exp\left(-\frac{x^2}{2R^2}\right) \tag{1}$$

to model the intensity distribution within the laser spot, where P_0 describe the temporal variation in pressure, x is spatial coordinate and R is the radius of the laser spot. Lateral plasma growth is accommodated by setting R to be three times larger its analog of the actual laser spot. The temporal aspect, follows previous work done on laser shocking of single crystals (Vukelić et al., 2009b) and is based on the work of Peyre et al. (2003) who measured the temporal pressure profile of laser pulses with 3 and 10 ns duration using VISAR (Velocity Interferometer System for Any Reflector) velocimetry technique (Peyre et al., 2003). Their study showed that an increase in duration of the laser pulse results in a decrease of peak pressure and an increase of full-width-at-half-maximum (FWHM). The temporal profile is used in the model as a semi-free parameter in order to match the experimental findings of displacement and lattice rotation. The initial yield stress is set to be 300 MPa and saturation stress 600 MPa following Peyre et al. (2003) and Nemat-Nasser et al. (1998).

The dynamic loading and wave propagation is characterized using a formulation based on the dynamic principle of virtual work (e.g. Hibbit et al., 1997; Zienkiewicz and Taylor, 2005)

$$\int_V \tilde{\tau} : \delta\tilde{\varepsilon}\, dV = \int_S \vec{t}\delta\vec{u}\, dS - \int_V \rho\frac{\partial^2\vec{u}}{\partial t^2}\delta u\, dV \tag{2}$$

where $\tilde{\tau}$ and $\tilde{\varepsilon}$ are any work conjugate pair of stress and strain tensor, $\vec{u}$ represents displacement and $\vec{t}$ is surface traction. In addition, V is the volume of the region under consideration and S is its surface area, $\delta\vec{u}$ is virtual displacement field and ρ is material density. At the end of each solution increment the main program passes to the UMAT the following variables: time increment, stress state, strain increment and solution dependent state variables ($s_i^{(\alpha)}, n_i^{(\alpha)}, \gamma^{(\alpha)}, g^{(\alpha)}$, etc.) defined by the user. The UMAT then updates the stress state and solution dependent variables and calculates material Jacobian matrix $\partial\sigma_{ij}/\partial\varepsilon_{kl}$. The new values are returned to solver, which applies the new stress state as a load increment and calculates the associated stain increment. Then process is iterated until the job is complete. More details about single crystal plasticity constitutive relations implemented in this model can be found in (Kysar, 2000; Vukelić et al., 2009a,b).

4. Results and discussion

4.1. Geometry of shocked region

The geometry of the surface prior to and after shocking was measured using an atomic force microscope (AFM) and stylus profilometer. Results from the AFM are shown in Fig. 4. The specimen was etched using sodium hydroxide before shocking to expose the grain boundary, so it is off interest to see if the chemical etched away a portion of the surface near the grain boundary that might affect the depth and shape of deformation. Fig. 4a shows that the surface roughness does not exceed 100 nm and that no distinctive groove due to etching is formed at the grain boundary. Similar conclusions can be drawn for reference baselines in single crystals, shown in Fig. 4b and c. Fig. 5 shows the geometric profile at the grain boundary from the profilometer measurements and in the reference single crystals after shocking as well as numerical results for the deformed geometry at the grain boundary. Several measurements along the shock lines have been performed giving similar results, which indicate that deformation is, to a good approximation, two-dimensional, with variability along the shock line about 15%. Numerical results for the grain boundary are given in Fig. 5b for comparison purpose whereas comparison between numerical analysis and experiments for single crystals case can be found elsewhere (Chen et al., 2004a,b; Wang et al., 2008; Vukelić et al., 2009a) and it will not be presented here. From Fig. 5a it can also be observed that depth of deformation close to the grain boundary is smaller than in reference single crystals.

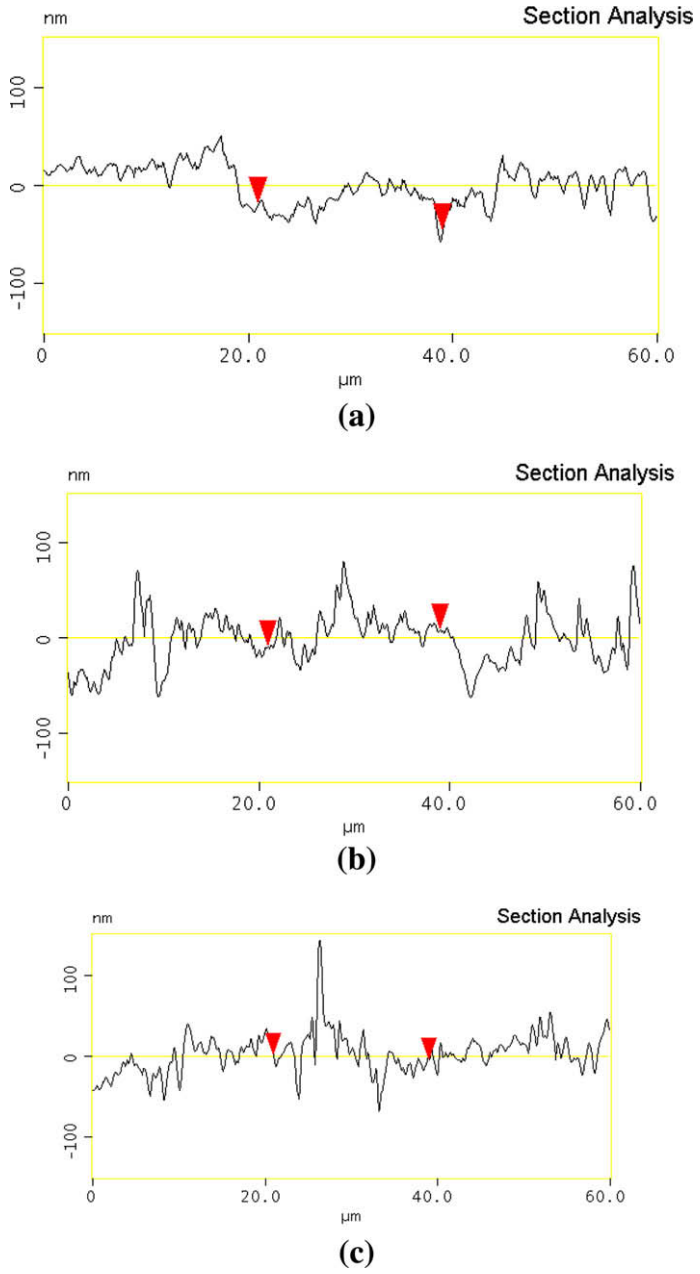

Fig. 4. Surface roughness – AFM measurements prior shocking: (a) grain boundary, (b) single crystal (110) and (c) single crystal (001).

Further it can be seen that the width of deformation is slightly wider close to the grain boundary of the bicrystal than in the single crystals. From Fig. 5b it can be seen that numerical simulation captures overall trend of the deformation, however it predicts much smaller values of displacement than seen in experiments. The discrepancy arises from assumptions in the numerical model which does not take into account shock wave propagation propagation in which equation of state governs the fluidlike material behavior (Fan et al., 2005). This was not used because one of our goals was to see how well the process can be modeled with only crystal plasticity. In addition, shear stresses at the interface of the coating layer and target material although expected to be small relative to pressure were not included in simulation Further, in the simulation loading is placed directly above the grain boundary which impedes propagation of plastic deformation. The results also indicate that the offset 70 μm into the interior of the (110) crystal due to backlash of the stage.

4.2. Electron backscatter diffraction

4.2.1. Inverse pole figures

Laser shocks cause plastic deformation that can be characterized by the change in the local crystallographic orientation obtained via electron backscatter diffraction (EBSD) measurements. One method to present the results is with inverse pole figures of the crystallographic orientation over the area of interest. An inverse pole figure of the untreated bicrystal at the grain boundary is shown in Fig. 6. The shocked reference single crystals of (110) and (001) orientation as well as μLSP treated grain boundary are shown in Fig. 7. The results show a definite change in crystallographic orientation after treating with μLSP as a consequence of lattice rotation. We can also observe that the change in crystallographic orientation is larger in the (110) crystal than in the (001) which is consistent with lattice rotation measurements shown in the following section.

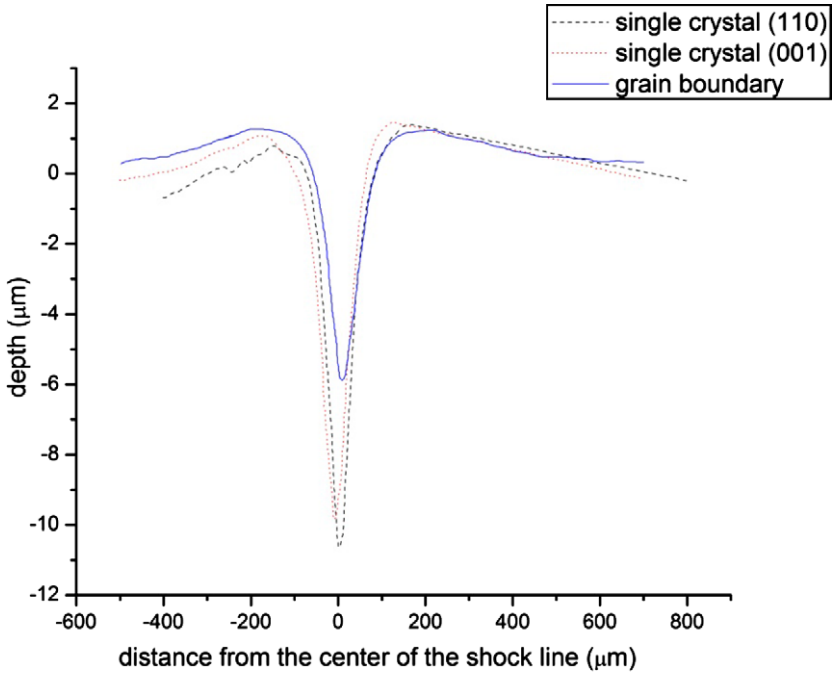

Fig. 5. Deformation geometry after shocking (a) experimental results (b) numerical results.

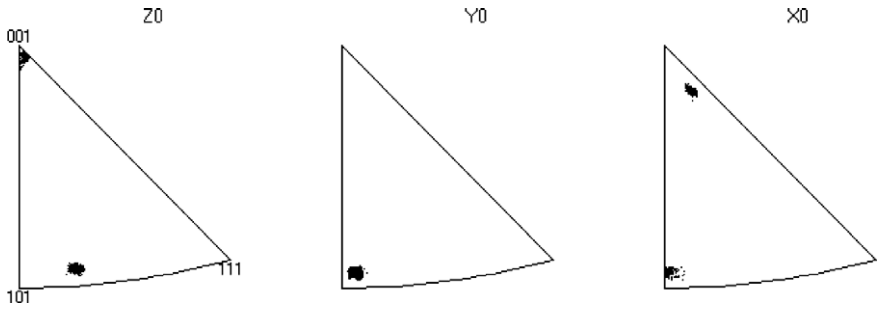

Fig. 6. Untreated bicrystal inverse pole figure.

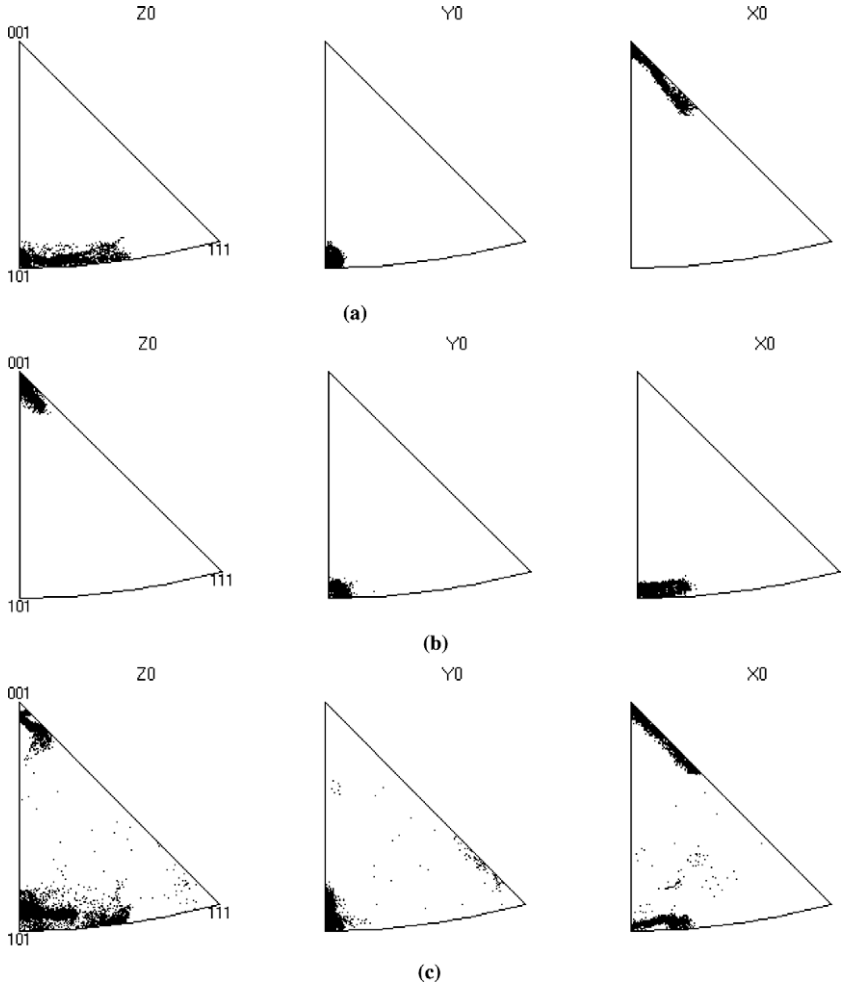

Fig. 7. Inverse pole figure after μLSP: (a) single crystal (1 1 0), (b) single crystal (0 0 1) and (c) grain boundary.

4.2.2. Lattice rotation of top surface

While the geometry of the deformation depends on the full deformation gradient tensor, ***F***, the lattice rotation is solely dependent on the evolution of the elastic part of ***F***. That is why is off interest to investigate lattice rotation which can further be compared with numerical analysis results for validation purpose. Maps of the crystal lattice rotation on the shocked surface of the reference single crystals and near the grain boundary of the bicrystal are shown in Fig. 8. Green regions represent rotation-free regions whereas other regions experienced a lattice rotation about the shock line (i.e. the *y*-axis) in the counter clockwise direction, as indicated by blue for clockwise rotated about the positive *y*-axis and by red for counter-clockwise rotation. For the bicrystal configuration, the clockwise rotation is associated with the $(1\bar{1}0)$ crystal while counter clockwise rotation is in the (0 0 1) crystal. From Fig. 8 it can be seen that deformation is fairly uniform along the shock line in both the bicrystal and reference single crystals indicating that approximate plane strain deformation states have been achieved. Deformation in the reference single crystal is, as expected, approximately symmetric because of the corresponding plastic yield loci corresponding to the (1 1 0) and (0 0 1) orientations (Rice, 1987; Kysar et al., 2005; Vukelić et al., 2009a). The deformation width is about 150 and 140 μm in the $(1\bar{1}0)$ and (0 0 1) case, respectively. Rotation in the $(1\bar{1}0)$ crystal is between −9° and 9° which is larger than the (0 0 1) where it ranges from −7° to 7°. Also it should be noted that the unrotated region of each shock line lies is much narrower for the $(1\bar{1}0)$ case than for the (0 0 1). The shocked, region near the grain boundary can be seen in Fig. 9c. Although the deformation appears similar to the single crystal references $(1\bar{1}0)$ and (0 0 1) suggesting the validity of the plane strain assumption, several differences should be noted. First, deformation is not symmetric with respect to the shock line. From Fig. 9c it can be observed that the green region (zero rotation) in the middle of the affected area is shifted toward the left with respect to the grain boundary. That is because laser shocks were applied close to the grain boundary, but not exactly at the grain boundary. Second, the magnitude of rotation at the bicrystal grain boundary is smaller than the rotation induced into the reference single crystals. When we compare the (0 0 1) reference single crystal and (0 0 1) crystal of the bicrystal we can see that the rotation is about 2° smaller in the bicrystal. An even larger discrepancy can be observed in the $(1\bar{1}0)$ crystal where the difference is about 4°. Less deformation may arise in the bicrystal because the grain boundary acts as an obstacle to the motion of dislocations and thus they pile up, making the nearby region harder to deform. Lastly, a discontinuity in lattice rotation can be observed at the grain boundary. The absolute magnitude of lattice rotation adjacent to the grain boundary from the $(1\bar{1}0)$ crystal is about 14° and on the other side of the grain boundary is 7°. The relative difference in lattice rotation across the grain boundary is approximately 1.5°.

4.2.3. Lattice rotation of cross-section

Lattice rotation maps of the cross-section of the bicrystal and reference (0 0 1) single crystal measured using electron backscatter

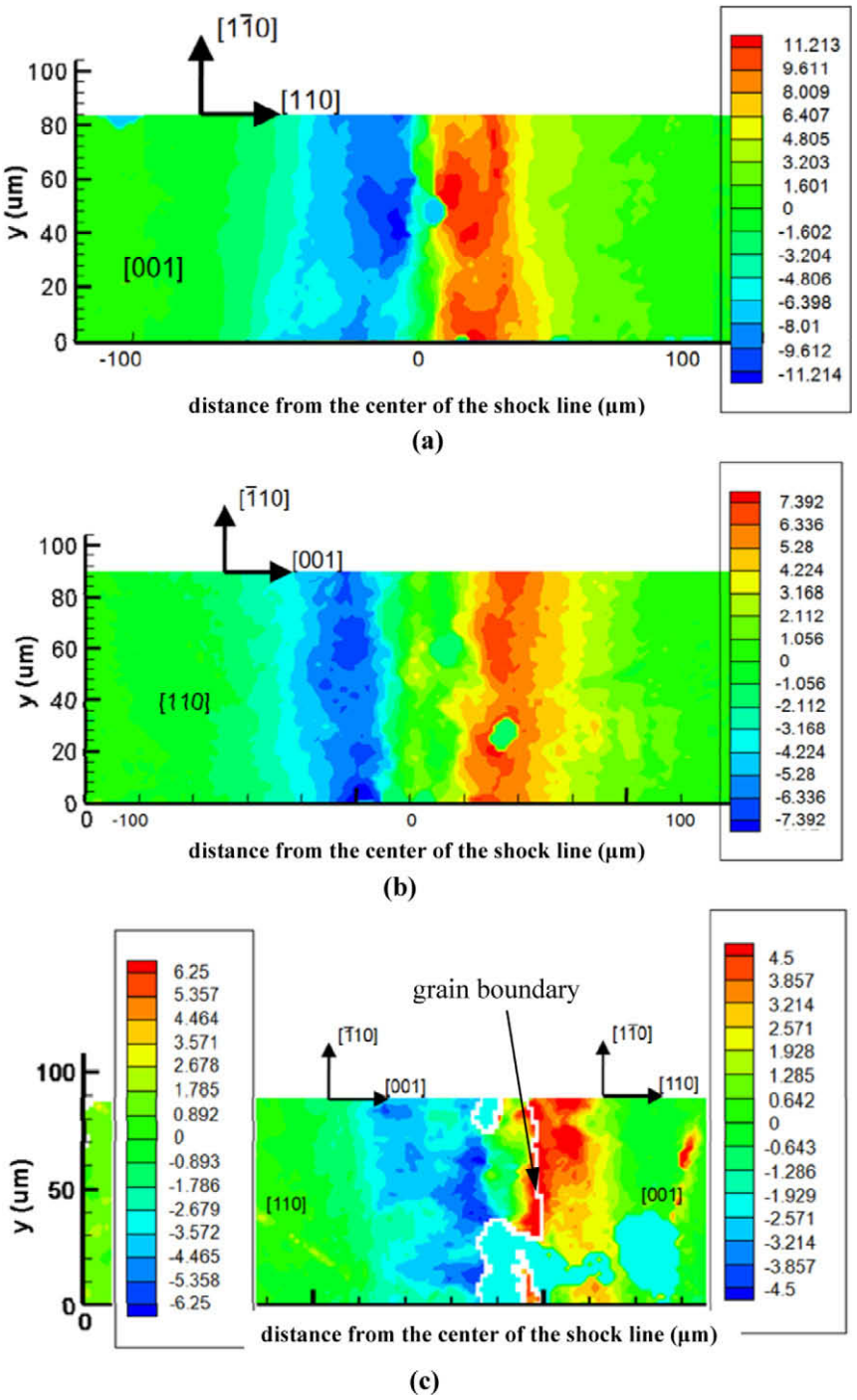

Fig. 8. Lattice rotation at the top surface: (a) single crystal (1 1 0), (b) single crystal (0 0 1) and (c) grain boundary.

rotation (EBSD) are shown in Fig. 9. Prior results for cross-section lattice rotation of the (1 $\bar{1}$ 0) crystal can be found in Vukelić et al. (2009a) and Chen et al. (2004a,b). From Fig. 9a it can be seen that the deformation width is approximately 160 μm which is consistent with top surface observations and depth of significant plastic deformation is about 50 μm. The lattice rotation pattern agrees very well with the finite element model of single crystal μLSP done by Chen et al. (2004a,b). The pattern is also symmetric which can be correlated with an analytic solution for plastic deformation under a Gaussian pressure distribution, discussed in detail for the (1 $\bar{1}$ 0) orientation single crystal aluminum in Vukelić et al. (2009a). Lattice rotation near the grain boundary is shown at Fig. 9b. Due to the backlash of stage used, the laser shock line was offset approximately 70 μm from the grain boundary within the (1 $\bar{1}$ 0) crystal interior, for the region chosen for the cross-section characterization. Thus it appears that the (0 0 1) crystal side of the grain boundary is only slightly affected by the shock peening. Fig. 9b shows a deformation width of about 90 μm which might be even larger because information close to the sample surface is lost due to the edge rounding during electropolishing of the specimen. The same statement applies to the deformation depth which appears to be approximately 50 μm, consistent with the reference single crystal results.

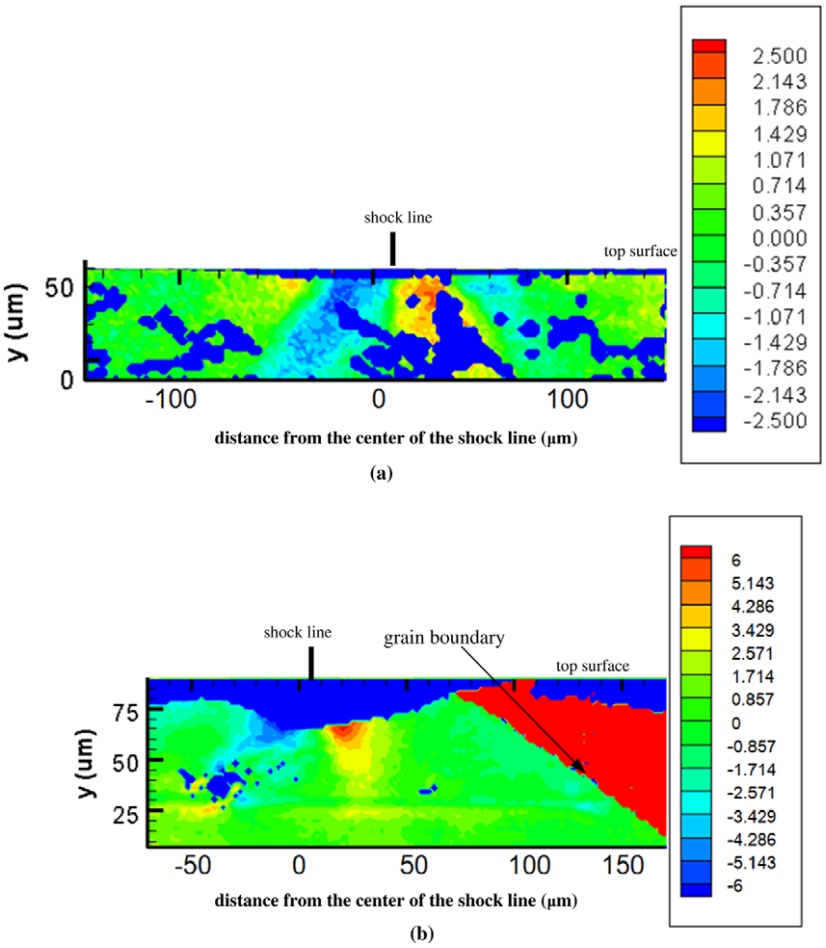

Fig. 9. Lattice rotation – cross-section: (a) single crystal (001) and (b) grain boundary.

Fig. 10. Numerical results – lattice rotation at grain boundary.

4.3. Numerical results

4.3.1. Lattice rotation

Numerical results for in-plane lattice rotation along the cross-section can be seen in Fig. 10. Results and discussion for the reference single crystals of $(1\bar{1}0)$ and (001) orientation can be found in Chen et al. (2004a,b) and Vukelić et al., 2009a,b, thus they will not be further elaborated upon here.

The magnitude of maximum rotation near the grain boundary is ±3.8° and the total deformation width is 90 μm and depth is 73 μm. Agreement between simulation and experiment is quite good, however some discrepancies should be noted. The depth of the affected region is larger in simulation than observed in experiments. The actual depth of significant plastic deformation may be larger than the experiments reveal, however because the edges of the speciment were slightly rounded during polishing. Second, the lattice rotation range at the grain boundary is smaller than seen in single crystals. This is likely because the grain boundary impedes plastic deformation leading to smaller rotation values. It should be noted that the width of deformation in the $(1\bar{1}0)$ is twice as large as the one in the (001). Also, although both crystallographic orientations have symmetric yield loci giving symmetric lattice rotation patterns in reference single crystals under Gaussian loading (Chen et al., 2004a,b; Vukelić et al., 2009a), the presence of the grain boundary plays a major role in case of the bicrystal. Non-symmetry of the domain of interest causes crystallographic lattice rotation to be non-symmetric with respect to the centerline of the shock, as seen in Fig. 10.

4.3.2. Shear strain increments

Numerical results for the shear strains on each active in-plane slip system are shown in Fig. 11a–c. There is total of three active in-plane slip systems and they are denoted as *i*, *ii* and *iii*. Details about active in-plane slip systems under plane strain conditions can be found in Rice (1987). The total accumulated shear in the aluminum bicrystal, are shown in Fig. 11d. Analogous results for the $(1\bar{1}0)$ and (001) orientations of aluminum single crystals under quasistatic loading are presented elsewhere (Chen et al., 2004a,b and Vukelić et al., 2009a) and the shear strains under dynamic loading are given in Vukelić et al. (2009b). The orientation of crystals in the bicrystal is such that the same slip systems are active and furthermore the yield loci have the same shape and orientation. However, the domain of interest is asymmetric due to the presence of the grain boundary, and one would intuitively assume that total shear strain field should indicate a lobe of deformation with higher magnitude in the right crystal where the slip direction does not point into the boundary. This is not the case, however, since it will become apparent, the effects of inertia are dominant over anisotropy. The earliest stages of deformation due to the pressure wave can be seen as analogous to elastic wave propagation in a mildly anisotropic media such as is used in non-destructive evaluation (NDE). Propagation of the elastic precursor precedes plastic deformation so the fields have similar shape. This analogy is applied to the single crystal case and explained in detail in Vukelić et al., 2009b. However, a jump discontinuity in total shear strain at the grain boundary exists, as seen in Fig. 11d. Further, Fig. 11c shows that the grain boundary does not have much impact on shear strain in slip system *ii*, which is similar to shear strain on the same slip system in the reference single crystals (Chen et al., 2004a,b; Vukelić et al., 2009a). On the other hand, it can be seen that the slips on slip systems *i* and *iii* experience a sharp discontinuity at the grain boundary. The portion most affected by the presence of the grain boundary is in the region directly beneath the Gaussian pressure loading as in the reference single crystal

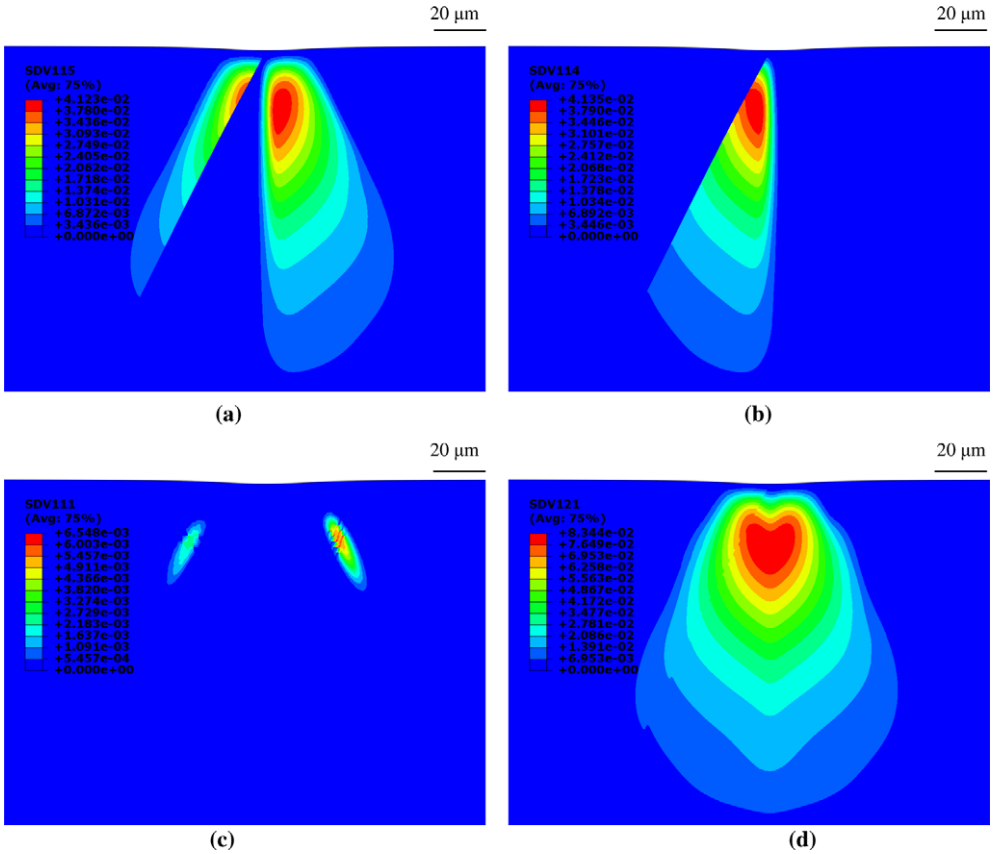

Fig. 11. Numerical results – shear strain increments: (a) shear strain increment *iii*, (b) shear strain increment *i*, (c) shear strain increment *ii* and (d) total shear strain increment.

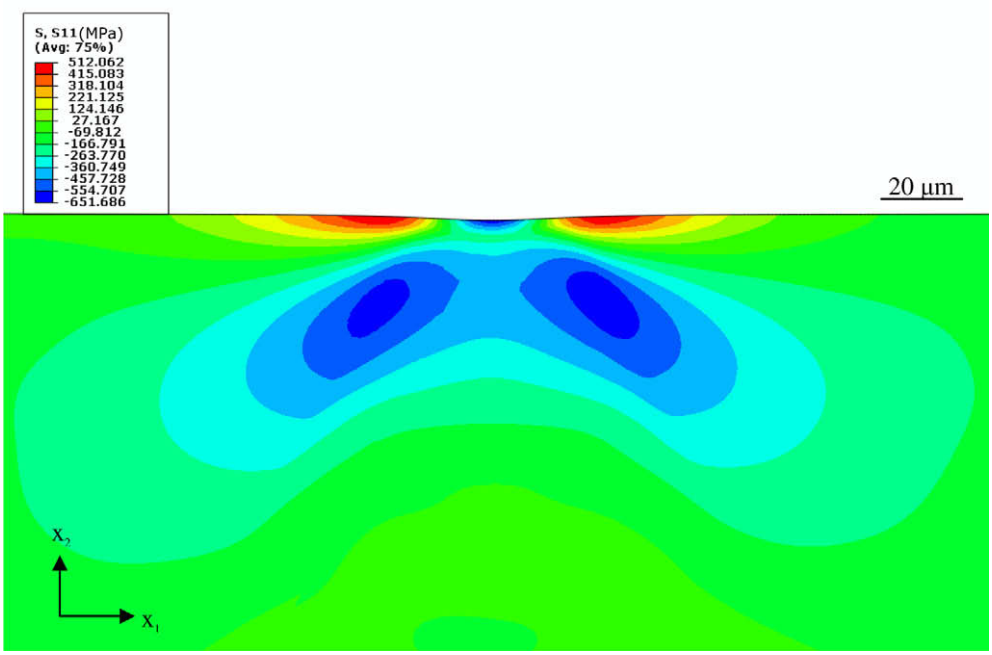

Fig. 12. Numerical results for residual stress distribution in 1–1 direction: (a) cross-sectional map and (b) averaged values.

(Vukelić et al., 2009b). The discontinuity is a consequence of an inability of the slip to transmit through grain boundary as well as a sudden change of resolved shear stress at the grain boundary, which introduces an effect analogous to the dislocation motion behavior mentioned in previously. Thus, plastic slip flows under compressive μLSP loading in each crystal until it reaches the grain boundary, which inhibits the plastic slip to be less than would otherwise occur in a single crystal.

4.3.3. Residual stress distribution

Wang et al. (2008) derived the analytical stress field distribution under a quasistatic loading in an elastic-ideally plastic single crystal aluminum with a $(1\bar{1}4)$ crystallographic orientation based on anisotropic slip line theory under Gaussian pressure loading. Vukelić et al. (2009a) derived the solution for the $(1\bar{1}0)$ case and made a comparison between single crystals of $(1\bar{1}0)$ and $(1\bar{1}4)$ orientation under the same conditions. Numerical results for the cases are given in references (Wang et al., 2008; Vukelić et al., 2009a) as well. In the case of dynamic loading, a numerical study has been performed for single crystals aluminum of the same orientations by Vukelić et al. (2009b), and the residual stress simulation results compared well with experimental findings.

Residual stress distribution for the σ_{11} stress component in x_1 direction is given at Fig. 12. From figure it can be seen that residual stress is continuous across the grain boundary as it must be and the stress field is fairly symmetric and compressive near the grain boundary. Tensile regions observed at the ends of the applied non-uniform pressure region are likely due to self-equilibration of the stresses. The stress distribution is similar to that of the $(1\bar{1}0)$ single crystal case (Vukelić et al., 2009b) and can be explained by the fact that both crystals in the bicrystal have symmetric yield loci resulting in the double slip case under μLSP. Small deviations from symmetry are due to the difference in angles between active slip systems axis for the $(1\bar{1}0)$ and (001) crystals. This is reasonable because elastic properties of aluminum single are almost isotropic.

4.3.4. Numerical results with offset load

It is of interest to perform finite element simulation μLSP with loading applied on the surface of the (001) crystal, close to the grain boundary to see how grain responds to the indirectly applied

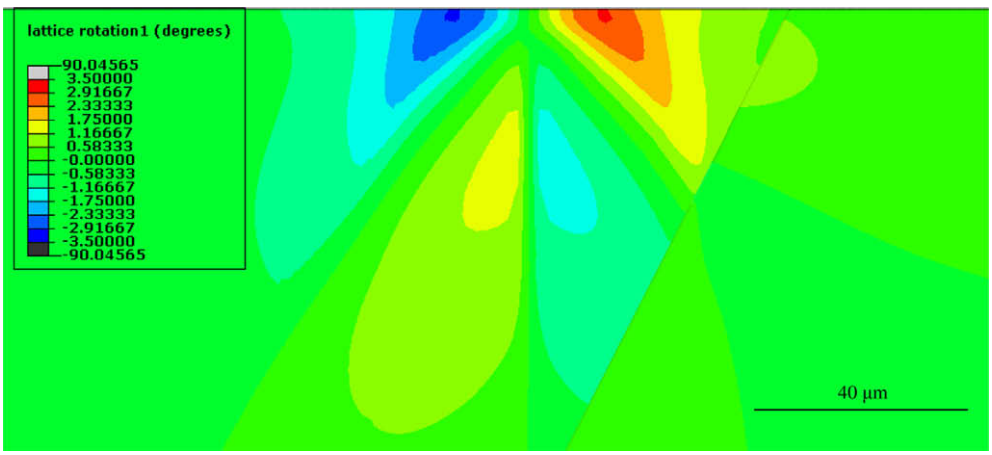

Fig. 13. Numerical results – lattice rotation induced by loading offset from the grain boundary into the (001) crystal by 50 μm.

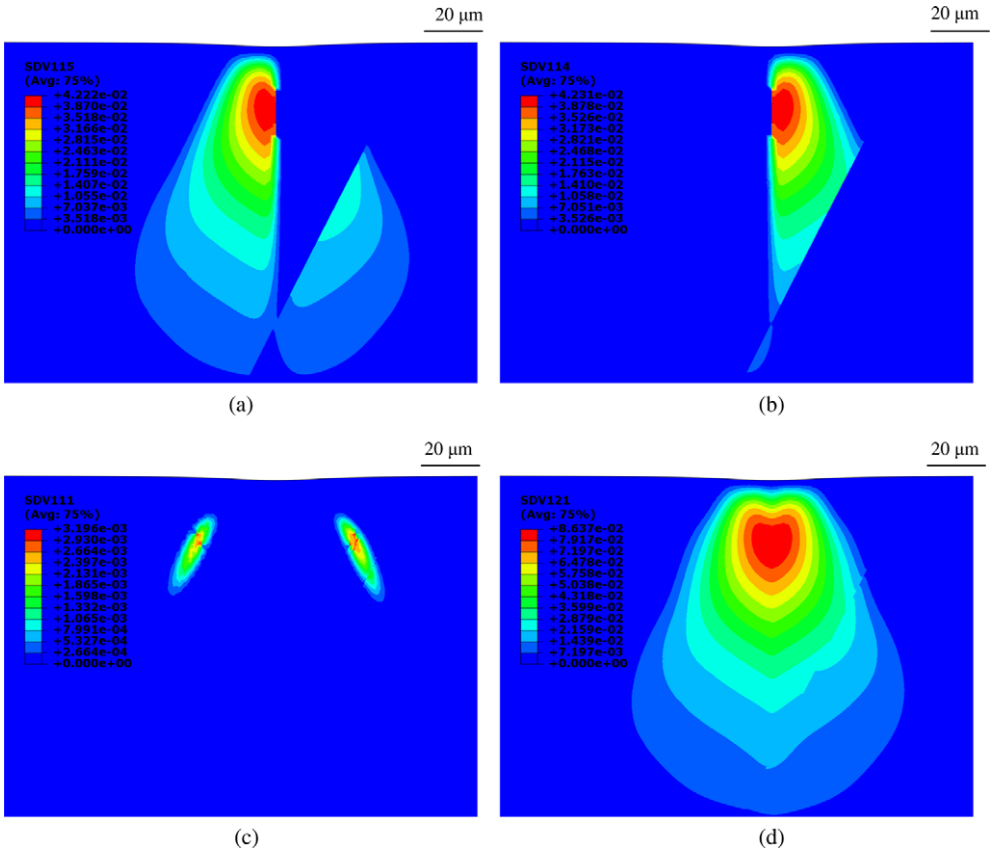

Fig. 14. Numerical results – shear strain increments induced by load offset from the grain boundary into the (001) crystal by 50 μm: (a) shear strain increment *iii*, (b) shear strain increment *i*, (c) shear strain increment *ii* and (d) total shear strain increment.

load. The (001) crystal is chosen because the grain boundary is inclined towards it and therefore as deformation propagates downwards it reaches the boundary. Figs. 13 and 14 depict lattice rotation and shear strain increment produced by a dynamic Gaussian pressure load applied 50 μm away from the grain boundary. From Fig. 13 it can be seen that although close to the boundary, the material response shows similar behavior as the single crystal (Vukelić et al., 2009b). There is very little impact on the adjacent grain, which is in good agreement with experimental findings shown above. Further, sharp discontinuity of plastic slip can be observed at the boundary, suggesting that no lattice rotation is transferred into the adjacent grain which is in line with results shown in previous sections. Shear strain increments at slip systems *i* and *iii* are different from the ones generated by Gaussian load applied directly at the grain boundary, as seen at Fig. 14a and b, whereas strain at the slip system *ii* is similar to it However, the most interesting result comes from the total slip (Fig. 14d). Here it can be seen that total deformation is essentially the same as that produced by the load applied directly onto the grain boundary. This indicates that inertial terms of the deformation are predominant and that anisotropy in case of dynamic load play minor role.

5. Conclusion

The behavior of a bicrystal aluminum as well as reference single crystals under Gaussian pressure loading have been presented in this study. Both, experimental and theoretical work was performed. Characterization of bicrystal and reference single crystals was done after applying μLSP. Smaller lattice rotations as well as a discontinuity in lattice rotation were observed near to the grain boundary and compared to the numerical model based on single crystal. Numerical results have shown that under Gaussian loading, the residual stress field is mostly compressive and therefore potential cracks at the grain boundary tend to close and which suggest that μLSP may be beneficial for extending fatigue life of components under cyclic loading. Moreover, when load is applied close to the grain boundary, but not exactly on it, the total plastic slip is approximately the same as in the case when loading is applied onto the boundary suggesting that inertia has plays a significantly more dominant role in establishing the details of the stress and deformation field than the anisotropy.

Acknowledgements

This work is supported under NSF CMMI-0500239, NSF-DMR-0706058, and NSF-CMMI-0826093. The authors would like to thank Dr. Paul van der Wilt for his great help and assistance in acquiring EBSD data.

References

ABAQUS Theory Manual, 1997. Hibbitt, Karlsson and Sorensen, Inc.
Asaro, R.J., 1983. Micromechanics of crystals and polycrystals. Advances in Applied Mechanics 23, 1–115.
Asaro, R.J., Needleman, A., 1985. Texture development and strain hardening in rate dependent polycrystals. Acta Metallurgica 33 (6), 923–953.
Chen, H., Wang, Y., Kysar, J.W., Yao, Y.L., 2007. Study of anisotropic character induced by microscale laser shock peening on a single crystal aluminum. Journal of Applied Physics 101, 024904-1–024904-8.
Chen, H., Yao, Y.L., Kysar, J.W., 2004a. Spatially resolved characterization of residual stress induced by micro scale laser shock peening. ASME Transactions Journal of Manufacturing Science and Engineering 126, 226–235.
Chen, H., Yao, Y.L., Kysar, J.W., 2004b. Characterization of plastic deformation induced by microscale laser shock peening. Journal of Applied Mechanics 71, 713–723.

Clauer, A.H., Holbrook, J.H., 1981. Effects of laser induced shock waves on metals. in: Shock Waves and High Strain Phenomena in Metals—Concepts and Applications. Plenum Press, New York, pp. 675–702.

Clauer, A.H., Lahrman, D.F., 2001. Laser shock processing as a surface enhancement process. Key Engineering Materials 197, 121–142.

Crone, W.C., Shield, T.W., Creuziger, A., Henneman, B., 2004. Orientation dependence of the plastic slip near notches in ductile FCC single crystals. Journal of the Mechanics and Physics of Solids 52, 85–112.

Curtis, S., de los Rios, E.R., Rodopoulos, C.A., Levers, A., 2002. Analysis of the effects of controlled shot peening on fatigue damage of high strength aluminum alloys. International Journal of Fatigue 25 (2003), 59–66.

Evers, L.P., Parks, D.M., Brekelmans, W.A.M., Geers, M.G.D., 2002. Crystal plasticity model with enhanced hardening by geometrically necessary dislocation accumulation. Journal of the Mechanics and Physics of Solids 50, 2403–2424.

Fan, Y., Wang, Y., Vukelić, S., Yao, Y.L., 2005. Wave–solid interactions in lasershock-induced deformation processes. Journal of Applied Physics 98 (10), 104904–104904-11.

Hall, E.O., 1951. The deformation and ageing of mild steel: III discussion of results. Proceedings Physical Society B 65, 747–753.

Hammersley, G., Hackel, L.A., Harris, F., 2000. Surface prestressing to improve fatigue strength of components by laser shot peening. Optics and Lasers in Engineering 34, 327–337.

Hill, R., 1950. The Mathematical Theory of Plasticity. Clarendon Press, Oxford.

Hook, R.E., Hirth, J.P., 1967. The deformation behavior of isoaxial bicrystals of Fe–3%Si. Acta Metallurgica 15, 535–551.

Huang, Y., 1991. A user-material subroutine incorporating single crystal plasticity in the ABAQUS finite element program. Mech. Report, 178, Division of Applied Sciences, Harvard University, Cambridge, MA.

Kysar, J.W., 1997. Addendum to a user-material subroutine incorporating single crystal plasticity in the ABAQUS finite element program. Mech. Report, 178, Division of Applied Sciences, Harvard University, Cambridge, MA.

Kysar, J.W., 2000. Continuum simulations of directional dependence of crack growth along a copper/sapphire bicrystal interface. Part I: Experiments and crystal plasticity background. Journal of the Mechanics and Physics of Solids 49 (2001), 1099–1128.

Kysar, J.W., Briant, C.L., 2002. Crack tip deformation fields in ductile single crystals. Acta Materialia 50, 2367–2380.

Kysar, J.W., Gan, Y.X., Mendez-Arzuza, G., 2005. Cylindrical void in a rigid-ideally plastic single crystal. Part I: Anisotropic slip line theory solution for face-centered cubic crystals. International Journal of Plasticity 21, 1481–1520.

Livingston, J.D., Chalmers, B., 1957. Multiple slip in bicrystal deformation. Acta Metallurgica 5, 322–327.

Ma, A., Roters, F., Raabe, D., 2006. A dislocation density based constitutive model for crystal plasticity FEM including geometrically necessary dislocations. Acta Materialia 54, 2169–2179.

Mesarevic, S.Dj., Kysar, J.W., 1996. Continuum aspects of directionally dependent cracking of an interface between copper and alumina crystals. Mechanics of Materials 23, 271–286.

Nemat-Nasser, S., Okinaka, T., Nesterenko, V., Liu, M.Q., 1998. Dynamic void collapse in crystals: Computational modeling and experiments. Philosophical Magazine A 78 (5), 1151–1174.

Petch, N.J., 1953. Cleavage strength of polycrystals. Journal of the Iron and Steel Institute 174, 25–28.

Peyre, P., Sollier, A., Chaieb, I., Berthe, L., Bartnicki, E., Braham, C., Fabbro, R., 2003. FEM simulation of residual stresses induced by laser peening. The European Physical Journal Applied Physics 23 (2), 83–88.

Rey, C., Zaoui, A., 1979. Slip heterogeneities in deformed aluminum bicrystals. Acta Metallurgica 28, 687–697.

Rice, J.R., 1973. Plane strain slip line theory for anisotropic rigid/plastic materials. Journal of the Mechanics and Physics of Solids 21, 63–74.

Rice, J.R., 1987. Tensile crack tip fields in elastic-ideally plastic crystals. Mechanics of Materials 6, 317–335.

Vukelić, S., Wang, Y., Kysar, J.W., Yao, Y.L., 2009a. Comparative study of symmetric and asymmetric deformation of Al single crystal under micro scale shock peening. Journal of Mechanics of Materials and Structures 4, 89–105.

Vukelić, S., Wang, Y., Kysar, J.W., Yao, Y.L., 2009b. Dynamic material response of aluminum single crystal under micro scale laser shock peening. Journal of Manufacturing Science and Engineering 131, 031015-1–031015-10.

Wang, Y., Kysar, J.W., Yao, Y.L., 2008. Analytical solution of anisotropic plastic deformation induced by micro-scale laser shock peening. Mechanics of Materials 40 (3), 100–114.

Wei, Y.J., Anand, L., 2004. Grain-boundary sliding and separation in polycrystalline metals: application to nanocrystalline fcc metals. Journal of the Mechanics and Physics of Solids 52, 2587–2616.

Zhang, W., Yao, Y.L., 2002. Microscale laser shock processing of metallic components. ASME Transactions on Journal of Manufacturing Science and Engineering (2), 369–378.

Zienkiewicz, O.C., Taylor, R.L., 2005. The Finite Element Method for Solid and Structural Mechanics. Elsevier.